JOURNAL OF THERMOPHYSICS AND HEAT TRANSFER
Vol. 8, No. 1, Jan.–March 1994

# Transient Conductive, Radiative Heat Transfer Coupled with Moisture Transport in Attic Insulations

R. Gorthala,* K. T. Harris,† J. A. Roux,‡ and T. A. McCarty§
*University of Mississippi, University, Mississippi 38677*

**A transient, one-dimensional thermal model that incorporates combined conduction, radiation heat transfer, and moisture transport for residential attic insulations has been developed. The governing equations are the energy equation, the radiative transport equation for volumetric radiation within the insulation batt, and the species equations for bound $H_2O$ and vapor $H_2O$. A simultaneous solution procedure with a Eulerian control volume-based finite difference method was used to solve the energy equation and the species equations. The method of discrete ordinates was used in solving the radiative transport equation. For $H_2O$ transport, both diffusion of vapor $H_2O$ and bound $H_2O$, and moisture adsorption/desorption within the insulation binder are included in the model. The experimental data measured at an occupied North Mississippi residence for R19STD (standard R19 fiberglass insulation batt without a foil radiant barrier) were used to validate the model which predicted heat fluxes for summer, spring, winter, and fall seasonal conditions. These predictions were compared with the measured heat flux data and the predictions from the dry model (without the moisture transport). Various profiles such as temperature-time histories, relative humidity time histories, spatial $H_2O$ concentrations, spatial temperatures, and spatial heat fluxes are presented to explain the overall heat transfer behavior.**

## Nomenclature

$c_f$ = specific heat, J/kg-K
$e_b$ = blackbody flux, W/m$^2$
$h_{ad}$ = heat of adsorption/desorption, J/kg
$I$ = radiative intensity, W/m$^2$-sr
$i_b$ = specific enthalpy of bound $H_2O$, J/kg
$i_v$ = specific enthalpy of vapor $H_2O$, J/kg
$k$ = thermal conductivity, W/m-K
$m_b$ = bound mass concentration, kg bound $H_2O$/m$^3$
$\dot{m}_b$ = rate of absorption of $H_2O$, Eq. (6), kg bound $H_2O$/m$^3$-s
$m_v$ = vapor mass concentration, kg vapor $H_2O$/m$^3$
$m_\phi$ = constant in Eq. (6b), Table 1
$n$ = refractive index of medium
$\dot{q}$ = source/sink term, W/m$^3$
$q_r$ = radiative component of total heat flux, W/m$^2$
$q_T$ = total heat flux, W/m$^2$
$RH$ = relative humidity
$T$ = temperature, K
$T_A$ = attic temperature, K
$T_C$ = ceiling temperature, K
$T_I$ = inside room temperature, K
$T_R$ = roof temperature, K
$T_r$ = reference temperature, 300 K
$T_S$ = bottom of the batt temperature, K
$T_0$ = top of the batt temperature, K
$t$ = time, s
$X$ = mass of absorbed moisture/mass of dry fiberglass, kg $H_2O$/kg fiberglass
$y$ = physical thickness, m
$y_0$ = thickness of insulation batt, m
$\beta$ = extinction coefficient, $\tau = \beta y$, cm$^{-1}$
$\gamma_b$ = diffusion coefficient of bound $H_2O$, m$^2$/s
$\gamma_v$ = diffusion coefficient of vapor $H_2O$, m$^2$/s
$\varepsilon_n$ = emissivity of the roof
$\varepsilon_s$ = emissivity of the substrate
$\theta$ = polar angle, deg
$\mu$ = cosine of polar angle
$\rho_f$ = density of fiberglass, kg/m$^3$
$\rho_n$ = reflectivity of the roof
$\rho_s$ = reflectivity of the substrate
$\tau$ = optical thickness
$\tau_0$ = optical thickness, $\beta y_0$
$\Phi$ = scattering phase function
$\phi$ = relative humidity
$\psi$ = azimuthal angle
$\omega$ = single scatter albedo

*Subscripts*
$b$ = bound
$f$ = fiberglass
$v$ = vapor
0 = top surface

Received Aug. 26, 1992; revision received March 9, 1993; accepted for publication March 11, 1993. 

*Graduate, Department of Mechanical Engineering. Member AIAA.
†Graduate Student, Department of Mechanical Engineering. Member AIAA.
‡Professor, Department of Mechanical Engineering. Member AIAA.
§Assistant Professor, Department of Mechanical Engineering.

## Introduction

With the constant depletion of energy sources, the need to explore renewable energy sources and conservation of energy have become very important. It should be realized that energy used for building heating and cooling represents a significant portion of the total national energy consumption in the U.S. If energy conservation is successfully applied to buildings, it can result in a significant reduction of the total energy consumption. To achieve this, identification of sources for energy conservation is crucial. It is well known that moisture has a pertinent effect on the energy required for cooling and heating buildings. It has been shown[1] that models used in energy analyses which do not account for moisture will not accurately predict both cooling loads and humidity conditions. The present work focuses on the study of heat transfer coupled with moisture transport in residential attic insulations. Once the model is developed and validated with experimental data, it can be used with prudent judgment to select the appropriate insulation with consideration of the local climatic conditions.

Simultaneous heat and mass transfer analysis is important in understanding the interaction of moisture transport with

transient heat transfer in different building porous insulation materials. Moisture transport is a very complex problem; various mechanisms of moisture transport are not unique for all porous insulations; they depend on the type of material, the density of the material, and the type of binder used with the material. There have been several works presented in the literature on porous insulations,[2-13] and a few works in particular on residential attic insulations. These works comprise laboratory experiments, in situ experiments, as well as mathematical models. Rish[2] developed a coupled conduction and radiation heat transfer model for dry residential attic insulations. Yeh[3] and Yajnik[4] presented works on radiative properties which are essential for heat transfer models. Much work has been done on simultaneous heat and mass transfer in porous insulations.[5-12] However, these works do not include volumetric radiative heat transfer within the material. A more recent work[13] did include the radiative component, but did not properly model the moisture adsorption and desorption. Also, Ref. 13 did not have sufficient data for boundary wet-bulb temperatures and had to parameterize those temperatures; in addition, Ref. 13 did not contain any winter, spring, or fall seasonal data for rigorous model verification.

Hence, the present study focuses on significantly expanding the model presented in Ref. 13, experimental validation of the improved model, and presenting other seasonal results. The present model comprises combined conduction, radiation heat transfer, and mass transfer. For the mass transfer analysis, the diffusion of both vapor $H_2O$ and bound $H_2O$ (inside the insulation phenolic binder) and an appropriate moisture adsorption/desorption model are included. The model includes a temperature-dependent vapor diffusion coefficient rather than a constant value as employed in Ref. 13. Effects of condensation and freezing are not considered since the climatic season conditions did not attain high enough relative humidities to result in condensation/freezing. The results for a standard fiberglass insulation (R19STD with an R-value of 3.3 m²K/W and 0.159-m thickness) are studied for summer, spring, fall, and winter situations.

## Statement of the Problem

Figure 1 shows a typical geometry for a residential home attic with the insulation batt placed above the gypsum board (ceiling). The characteristic variables describing the attic thermal environment are denoted by $T$ and $RH$. The boundaries for the fiberglass insulation are air at the top and a gypsum board (ceiling) at the bottom. As seen in Fig. 1, the coordinate system is placed at the substrate with $y = 0$ at the substrate, and $y = y_0$ ($y_0 = 0.159$ m) at the top of the insulation.

Considering the various heat transfer mechanisms that are present in the attic environment, conduction and radiation heat transfer are the obvious and primary mechanisms. Ac-

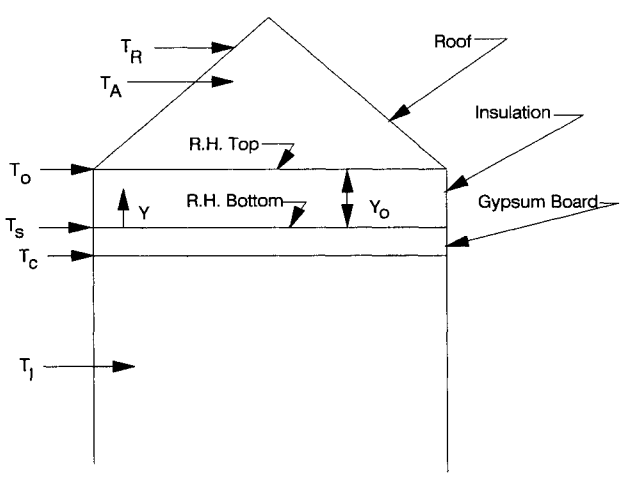


**Fig. 1 Attic geometry.**

**Table 1 Radiative and thermal properties used in numerical computations**

| | |
|---|---|
| $\rho_f$ | 12, kg/m³ |
| $c_f$ | 844.4, J/kg-K |
| $k_f$ | $a + bT + 8.5537 \times 10^{-5}\ \rho_f$, W/m-k |
| | $a = 4.97576 \times 10^{-3}$, $b = 7.00025 \times 10^{-5}$ |
| $\omega$ | 0.201 |
| $\beta$ | 3.7, cm⁻¹ |
| $\gamma_{vR}$ | $1.2 \times 10^{-5}$, m²/s |
| $\gamma_b$ | $1.185 \times 10^{-9}$, m²/s |
| $m_\phi$ | 1/100 $0.10 \le \phi \le 0.90$ |
| $\gamma_v/\gamma_{vR}$[17] | $(T/T_r)^{1.5}$ |

cording to Rish,[2] radiation can account for about 45% of the total heat transfer. Besides these two mechanisms, other possible transport mechanisms are caused by the presence of moisture in the attic air. This moisture presence in the attic air and in the fiberglass insulation phenolic binder are expected to influence the overall heat transfer. It is considered that moisture exists inside the insulation in two forms: 1) one is in the vapor $H_2O$ form and is free to diffuse under vapor concentration gradients; and 2) the other is in the form of bound $H_2O$ inside the insulation binder. If the relative humidities and the temperatures are different at the top and bottom of the insulation, there will be concentration gradients for the vapor $H_2O$ and the bound $H_2O$; hence, mass diffusion will occur. As these species diffuse through the insulation, energy (enthalpy) is carried with the associated species. Also, a change in temperature and relative humidity with time can result in the adsorption/desorption of moisture from within the insulation binder. When desorption takes place, bound $H_2O$ becomes free vapor $H_2O$, and the insulation acts as a heat sink and loses heat through desorption. It was shown in Ref. 12 that adsorption and desorption isotherms are not identical and that there is a small hysteresis phenomenon present. This study assumes that adsorption and desorption follow the same path and that the hysteresis is negligible. The data presented[12] is for fiberglass with a density of 18 kg/m³ at 20°C. Only adsorption isotherm data were presented in Ref. 8 for different temperatures for fiberglass with a density of 101 kg/m³. However, the density of the fiberglass insulation used in this study is 12 kg/m³.[14] Since there is very little adsorption/desorption data available for the present insulation, the most pertinent data available[12] is used for modeling adsorption/desorption. The heat of adsorption and desorption may not be the same as the heat of vaporization[10,11]; they are functions of moisture content and can be as high as a factor of 4 compared to the heat of vaporization. However, the heat of adsorption was reported to be equal to the heat of vaporization when moisture content was greater than 0.1 wt %. The applicable data used in the present model[10,11] indicate that the mixture content is always greater than 0.1 wt %. Therefore, the heat of adsorption/desorption can be assumed to be equal to the heat of vaporization. The temperatures at the insulation top, bottom, and roof are the required boundary condition information for solving the energy equation and radiative transport equation. The boundary temperatures and relative humidities are required for obtaining concentrations of $H_2O$ species which are needed for solving the species equations. Emissivities are specified at the roof ($\varepsilon_n = 1 - \rho_n = 0.85$) and substrate ($\varepsilon_s = 1 - \rho_s = 0.93$) surfaces.[3] Thermal/radiative properties in this model are presented in Table 1.

## Analysis

Because attic insulation behaves like a plane parallel layer, the complexity of the problem is reduced by considering it to be one-dimensional. The governing equations appropriate for this problem are the energy equation, the species equations for bound $H_2O$ and vapor $H_2O$, and the radiative transport equation. The assumptions made in the development of this model are given as follows: 1) transient, one-dimensional

combined conduction, radiation heat transfer with diffusion, and adsorption/desorption of bound $H_2O$ and vapor $H_2O$; 2) volumetric radiation within the fiberglass insulation with absorbing, emitting, and scattering (isotropic) medium; 3) gray radiative properties (extinction coefficient and albedo); 4) convection of vapor is neglected; and 5) relative humidities and temperatures at the boundaries are known (measured) functions of time.

**Energy Equation**

The one-dimensional energy equation for transient, coupled conduction, radiation heat transport, diffusion of vapor $H_2O$ and bound $H_2O$, and adsorption/desorption of moisture is given by

$$\frac{\partial}{\partial y}\left(k_f \frac{\partial T}{\partial y}\right) - \frac{\partial q_r}{\partial y} + \frac{\partial}{\partial y}\left(\gamma_v i_v \frac{\partial m_v}{\partial y}\right) + \frac{\partial}{\partial y}\left(\gamma_b i_b \frac{\partial m_b}{\partial y}\right) + \dot{q} = \rho_f c_f \frac{\partial T}{\partial t} \tag{1a}$$

where

$$\dot{q} = h_{ad}\dot{m}_b \tag{1b}$$

with boundary conditions

$$T = T_s(t) \quad \text{at} \quad y = 0$$

$$T = T_0(t) \quad \text{at} \quad y = y_0$$

and a linear temperature profile was chosen as the initial temperature condition (midnight, $t = 0$).

The terms on the left side of the Eq. (1a) represent heat conduction, radiation, diffusion of vapor $H_2O$ and bound $H_2O$, and the heat source/sink due to $H_2O$ adsorption/desorption within the insulation, respectively; whereas the term on the right side represents the transient (internal energy) term.

**Radiative Transport Equation**

The radiative heat flux $q_r$ is required for solving Eq. (1a); it is obtained by solving the radiative transport equation as presented below. The one-dimensional axially symmetric radiative transport equation for an absorbing, emitting, and anisotropically scattering medium from Ref. 15 can be written as

$$\mu \frac{dI(\tau, \mu)}{d\tau} = -I(\tau, \mu) + \frac{\omega}{2}\int_{-1}^{1} I(\tau, \mu')\Phi(\mu, \mu')\, d\mu' + n^2(1 - \omega)I_b[T(\tau)] \tag{2}$$

It is assumed here that $\Phi$ is equal to 1 for isotropic scattering.

The boundary conditions for the Eq. (2) are given by

$$I(0, \mu) = \rho_s I(0, -\mu) + (1 - \rho_s)n^2 I_b(T_s), \qquad \mu > 0$$

$$I(\tau_0, -\mu) = \rho_n I(\tau_0, +\mu) + (1 - \rho_n)n^2 I_b(T_R), \qquad \mu > 0$$

where $I_b(T_R) = e_b(T_R)/\pi$, and for a gray body $e_b(T_R) = \sigma T_R^4$. It should be noted that $n = 1$ for this problem. A quasi-analytical technique with the method of discrete ordinates, employing a 16-point Gaussian quadrature, was used in solving the radiative transport equation [Eq. (2)], and the details can be found in Refs. 2, 3, and 15. The radiative heat flux needed in Eq. (1a) is given by definition as

$$q_r(\tau) = \int_0^{2\pi}\int_{-1}^{1} I(\tau, \mu)\mu\, d\mu\, d\psi \tag{3}$$

**Species Equations**

For one-dimensional unsteady moisture transport, the species conservation equation for bound $H_2O$ can be expressed as

$$\frac{\partial m_b}{\partial t} - \frac{\partial}{\partial y}\left(\gamma_b \frac{\partial m_b}{\partial y}\right) = \dot{m}_b \tag{4}$$

Here, $\dot{m}_b$ is the source/sink term. Similarly, the species conservation equation for vapor $H_2O$ can be written as

$$\frac{\partial m_v}{\partial t} - \frac{\partial}{\partial y}\left(\gamma_v \frac{\partial m_v}{\partial y}\right) = \dot{m}_v \tag{5}$$

In the above equation, all the terms denote the same meaning as in Eq. (4), except that the subscript "$v$" denotes vapor $H_2O$. The source terms ($\dot{m}_b$, $\dot{m}_v$) in Eqs. (4) and (5) account for $H_2O$ adsorption/desorption. It should be noted that the adsorption rate of bound $H_2O$ is equal to the desorption rate of vapor $H_2O$ and vice versa. Therefore, the source term is given by

$$\dot{m}_b = -\dot{m}_v = \rho_f \frac{\partial X}{\partial t} \tag{6a}$$

where

$$\frac{\partial X}{\partial t} = m_\phi \frac{\partial \phi}{\partial t} \tag{6b}$$

In Eq. (6b), $m_\phi$ is a constant obtained from the data presented in Ref. 12, and is given in Table 1. The symbol $\phi$ is relative humidity and Eqs. (6a) and (6b) yield the moisture adsorption/desorption as a function of the relative humidity in accordance with Ref. 18, which reported the adsorption isotherm to be a function of relative humidity only, and not a separate function of temperature. The boundary conditions for Eqs. (4) and (5) are given by

$$m_b = (m_b)_s(t); \quad m_v = (m_v)_s(t) \quad \text{at} \quad y = 0$$

$$m_b = (m_b)_0(t); \quad m_v = (m_v)_0(t) \quad \text{at} \quad y = y_0$$

These concentrations were determined from the measured relative humidity and temperature at the substrate and top of the insulation batt. Linear vapor $H_2O$ and bound $H_2O$ concentration profiles were chosen as the initial concentration conditions (midnight, $t = 0$). Equation (7) yields the total heat flux

$$q_T = -k\left(\frac{\partial T}{\partial y}\right)_{y=0} + q_r(0) - \gamma_v\left(\frac{\partial m_v}{\partial y}\right)_{y=0} i_v - \gamma_b\left(\frac{\partial m_b}{\partial y}\right)_{y=0} i_b \tag{7}$$

Equations (1–6) were solved simultaneously by an iterative scheme that employs a control volume-based finite difference method[16] which was used in Refs. 2, 3, and 13. The transient solution is obtained by marching forward in time with an appropriate time step (5-min time step). The largest time step that yielded no change in the converged temperatures and species was considered the appropriate time step. A non-uniform grid with 17 nodal points was used in the program to achieve lower computational time without sacrificing accuracy[3]; the computation time on an IBM 3084 to predict all the results for a 24-h period was about 60 s of CPU time. It should be noted that the experimental data obtained were recorded every 15 min, and therefore, a linear interpolation

was used to input boundary condition information at the 5-min time step intervals which occur in between the 15-min data acquisition intervals for experimental data.

## Results

The heat transfer results are presented as a comparison between the numerically predicted total heat fluxes [Eq. (7)] and the experimentally measured total heat fluxes. Comparisons are made for a wide variety of seasonal conditions. However, the results presented here are for representative comparisons between the numerical model and the experimental data; these results are separated into summer, spring, fall, and wintertime comparisons.

### Summer Conditions

The summer conditions correspond to the data recorded during the 24-h time period of June 27, 1992. Shown in Fig. 2 are the temperature-time histories. As explained earlier, the roof temperatures, top of the batt temperatures, and bottom of the batt temperatures are employed as boundary condition information for the numerical model. The roof ($T_R$) is seen to reach a high temperature, and radiates a high heat flux to the insulation batt. Due to this radiative flux, the top ($T_0$) of the batt is seen to reach a higher temperature than the attic air ($T_A$) at 0.0508 m (2 in.) above the batt. The substrate ($T_S$) and inside ceiling ($T_C$) temperatures are quite close to one another as expected, and cross in magnitude depending on whether heat is entering (negative heat flux) or leaving (positive heat flux) the living space through the ceiling.

Shown in Fig. 3 are the measured relative humidity time histories for both summer and winter conditions. In the summer the relative humidity routinely reached the upper 70s in the attic at the top of the insulation batt, even though the outdoor relative humidity reached values up to the low 90s in the morning ($t \approx 300$ min); this is because the wood and fiberglass binder act to absorb moisture during the night from the attic air. The relative humidity at the substrate in the summer varied during the day from about 37 to about 45%. Using the measured temperatures and relative humidities from Figs. 2 and 3, the dimensionless ($m_v/\rho_f$) vapor $H_2O$ concentrations are presented in Fig. 4. It can be seen from Fig. 4 that for June 27, 1992 the vapor concentration at the top of the batt was always greater than at the substrate, and hence, there was always a diffusion of vapor $H_2O$ from the top to the bottom of the insulation batt. The vapor concentration is significantly higher at the top of the batt during the high roof temperature portion of the day; this is due to $H_2O$ desorption both from the insulation batt and from the attic wooden components such as the roofing boards. The information shown in Fig. 4 was employed as the boundary conditions for the vapor $H_2O$ species equation [Eq. (5)]. The bound $H_2O$ concentration is essentially the same as given by Eq. (6b) since the bound $H_2O$ diffusion coefficient is essentially zero [$\approx O(10^{-9})$].

With the above temperatures and concentrations employed as boundary condition information, the total predicted and measured heat fluxes are compared in Fig. 5. Presented in Fig. 5 are the experimental data, the numerical model with moisture (MOIST), and the numerical model with no vapor

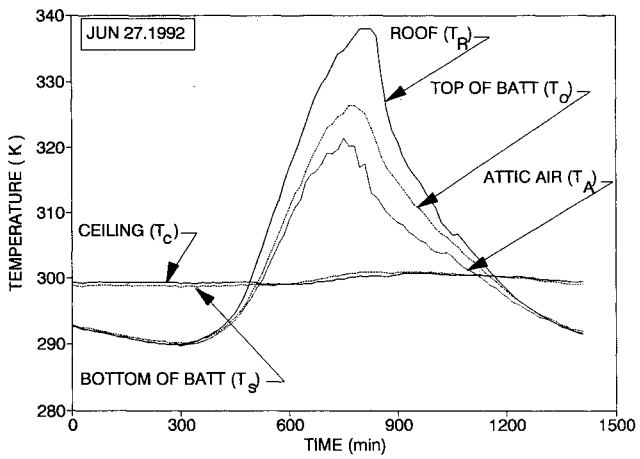


**Fig. 2 Temperature-time histories data for R19STD insulation for June 27, 1992.**

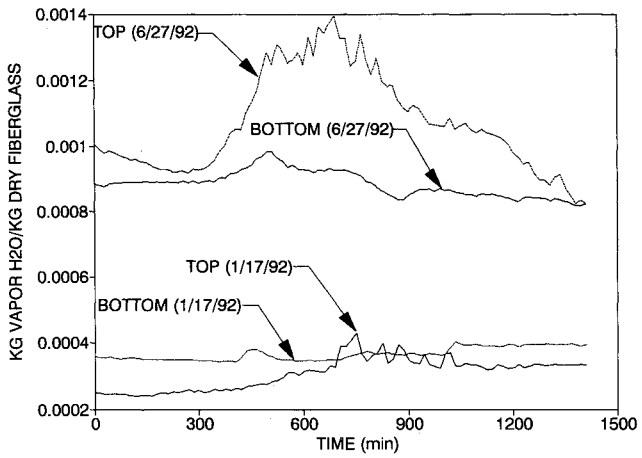


**Fig. 4 Vapor $H_2O$ concentration histories for both summer and winter conditions at different locations of the batt for R19STD insulation.**

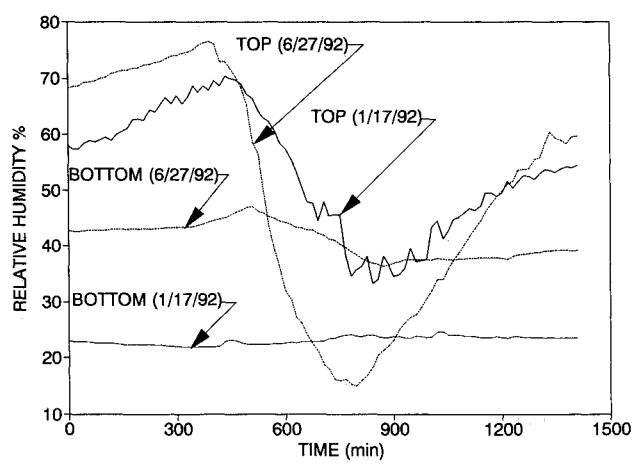


**Fig. 3 Measured relative humidities at different locations of the batt for both summer and winter conditions for R19STD insulation.**

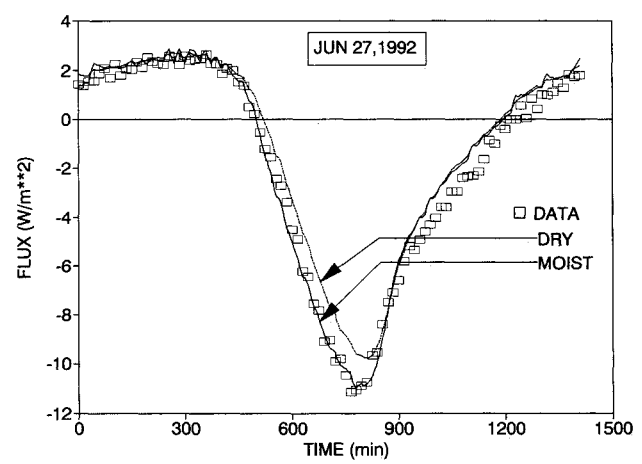


**Fig. 5 Substrate measured heat flux-time and predicted heat flux-time histories for both moist and dry cases for R19STD insulation.**

**Table 2 Time integrated substrate heat flux corresponding to R19STD fiberglass for summer, fall, and winter conditions**

| Date | Experimental data, kJ/m² | Dry model, kJ/m² | Moist model, kJ/m² | Difference I,[a] % | Difference II,[b] % | Difference III,[c] % |
|---|---|---|---|---|---|---|
| 6/27/92[d] | −62.6 | −51.5 | −60.1 | 17.7 | 4.1 | 14.2 |
| 1/17/92[e] | 122.4 | 112.1 | 115 | 8.4 | 6.1 | 2.5 |
| 10/8/92[f] | −8.1 | −6.6 | −7.9 | 17.7 | 1.1 | 16.7 |

[a]Difference I, between experimental data and dry model. [b]Difference II, between experimental data and moist model. [c]Difference III, between dry model and moist model. [d]Integrated over heat gain period ($530 < t < 1180$ min). [e]Integrated over heat loss period (24 h). [f]Integrated over heat gain period ($620 < t < 910$ min).

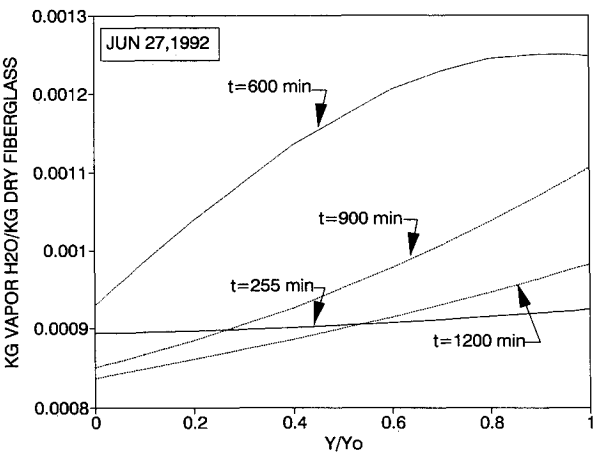


**Fig. 6 Spatial vapor $H_2O$ concentration (kg $H_2O$/kg of dry fiberglass) profiles at four times for R19STD insulation.**

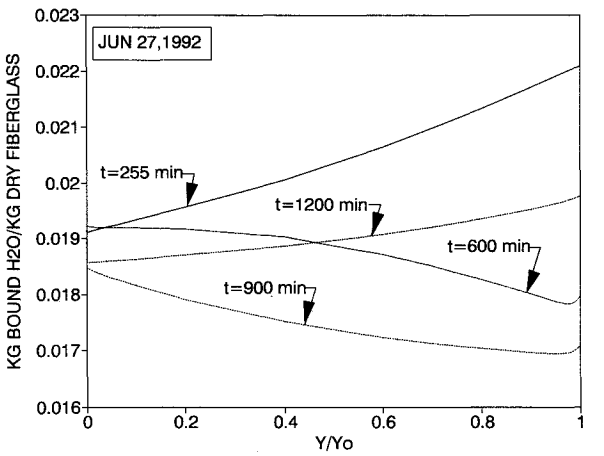


**Fig. 7 Spatial bound $H_2O$ concentration (kg $H_2O$/kg dry fiberglass) at four times for R19STD insulation.**

$H_2O$ or bound $H_2O$ consideration (DRY). In the early morning it is seen that all three agree quite well. However, when the heating period (≈450–1100 min) begins, the dry model starts to deviate from the experimental data and underpredicts the peak heating (≈800 min). The moist model, however, shows very good agreement with the experimental heat flux data and matches the peak heating very well. The difference in the predicted heat transfer between the moist and dry models is due primarily to the coupled effects of vapor $H_2O$ diffusion and $H_2O$ desorption/absorption of the phenolic insulation binder. As the magnitude of the heat transfer into the living space (negative sign) decreases, the dry and moist models begin to agree (≈900 min) with one another, but show some small disagreement with the experimental data. For the moist model this could be due to the possible hysteresis phenomenon between adsorption and desorption which is not well characterized experimentally or modeled in this work. The integrated heat fluxes for the three cases are presented in Table 2. It can be seen from Fig. 5 and Table 2 that the presence of moisture has resulted in a 14.2% increase in the heat transfer as compared to the dry model during the heating (negative flux) period of the day for 6/27/92. The downward diffusion of vapor $H_2O$ has provided an additional mode of heat transfer as compared to the dry model. The moist model is seen to agree within 4% of the experimental data. Shown in Fig. 6 are the dimensionless $H_2O$ vapor concentration spatial profiles at various times during the day; the parameter $y/y_0$ is the dimensionless distance from the bottom to the top of the batt. The value of $y_0$ is 0.159 m (6.25 in.). The vapor concentration at $t = 600$ min shows a nonmonotonic behavior and is due to the desorption of vapor $H_2O$ near the top of the batt; this vapor both diffuses down to the substrate and diffuses out to the top of the insulation. The vapor concentrations at the other times are monotonic as expected. The vapor concentration spatial profile at $t = 255$ min is essentially constant, as also inferred from Fig. 4.

Depicted in Fig. 7 are the dimensionless bound $H_2O$ concentration profiles. In accordance with the findings of Ref. 18, these profiles are a function of the local relative humidity. The dip in the curves at $t = 600$ and 900 min are due to the desorption of $H_2O$ at the higher temperatures near the top of the batt.

### Spring Conditions

Spring conditions correspond to the data recorded during the 24-h time period of May 24, 1992. Similar temperature-time histories and relative humidity histories were developed as in Figs. 2 and 3, respectively, but are not shown. It should be noted that this was a cloudy, rainy day with the roof temperature not exceeding 80°F and the relative humidity inside of the attic averaging about 65%, making this a very mild and humid day. The dimensionless $H_2O$ vapor concentrations are presented in Fig. 8. Figure 8 depicts that for most of the 24-h time period on May 24, 1992, the vapor concentrations were higher at the top of the batt than those at the bottom of the batt, which would cause $H_2O$ vapor to diffuse downward. Therefore, this diffusion of vapor would carry enthalpy with it, and this enthalpy is a form of energy transport. Figure 9 shows the heat-flux time histories for May 24, 1992. It can be seen that the moist numerical model agrees with the data throughout the 24-h time period. Once again, the coupled effects of vapor $H_2O$ diffusion and $H_2O$ desorption/absorption of the phenolic binder causes the difference between the dry and moist models. With the presence of moisture the numerical model shows a significant increase in the overall heat transfer in comparison to the dry model. These spring results are not compared in Table 2, since during the heating portion of the day ($600 < t < 1130$ min) the dry model shows heat leaving the house (positive flux) and the moist model shows heat entering the house (negative flux) (Fig. 9).

### Winter Conditions

Winter conditions correspond to the data recorded during the 24-h time period of January 17, 1992. The temperature-time histories for this day are shown in Fig. 10. As seen, the bottom of the insulation ($T_S$) is at a lower temperature than

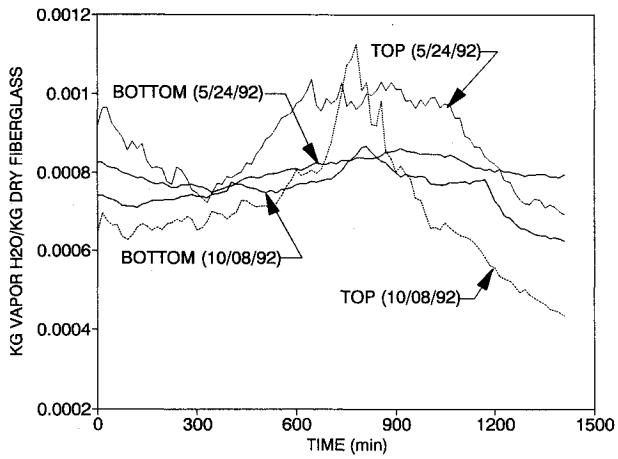


Fig. 8 Vapor $H_2O$ concentration histories for both spring and fall conditions at different locations of the batt for R19STD insulation.

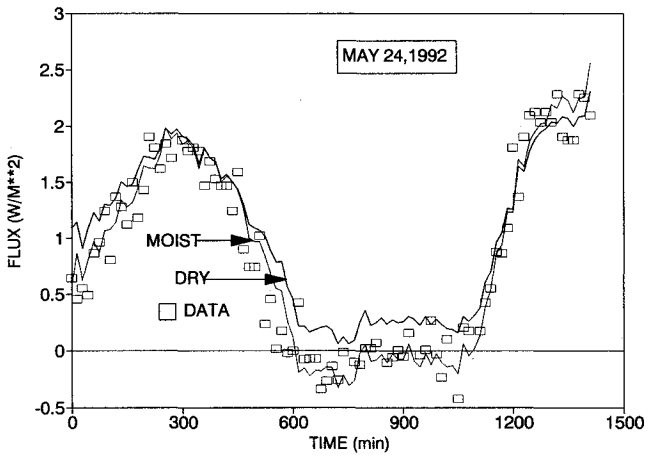


Fig. 9 Substrate measured heat flux-time and predicted heat flux-time histories for both moist and dry cases for R19STD insulation.

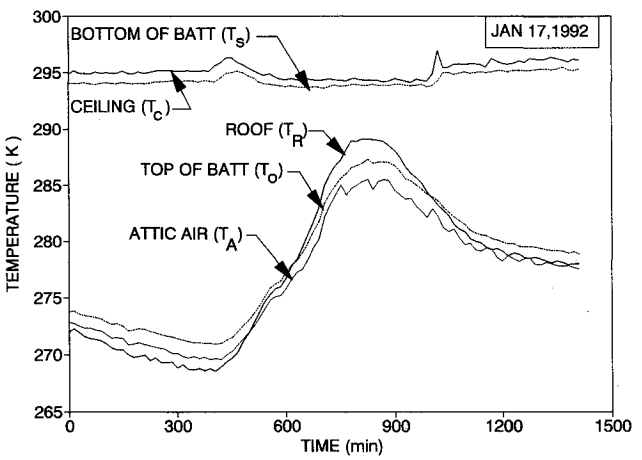


Fig. 10 Temperature-time histories data for R19STD insulation for January 17, 1992.

the conditioned space ($T_C$) during the entire day. The roof temperature is the lowest during the early morning hours ($t < 400$ min), but increases during the day as a result of solar heating. However, the roof, attic air, and top of the insulation temperatures remain substantially lower than the bottom of the insulation temperature during the entire day. Therefore, under these conditions, heat was lost (Fig. 11) during the entire day. The relative humidity-time histories for this winter day are shown in Fig. 3. The relative humidity at the top of

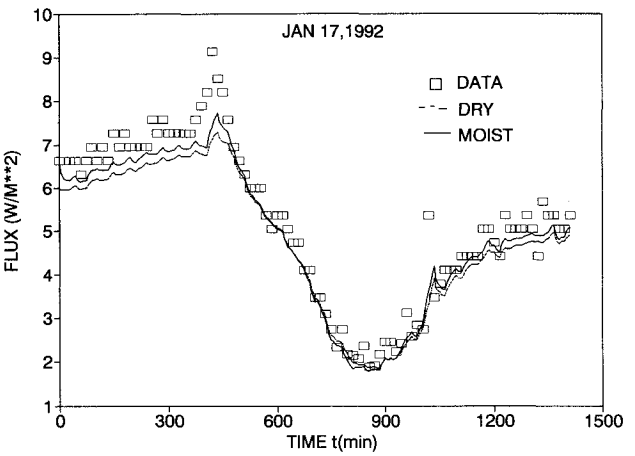


Fig. 11 Substrate measured heat flux and predicted heat flux-time histories for both moist and dry cases for R19STD insulation.

the batt does not rise quite as high in winter as it does in summer, and also, it does not decrease as much during the middle of the day as it does in summer. Using the temperature data from Fig. 10 and the relative humidity from Fig. 3, the vapor $H_2O$ dimensionless concentration histories are shown in Fig. 4 for the top and bottom of the insulation for winter conditions. The vapor $H_2O$ concentration histories are relatively flat in comparison to the summertime vapor $H_2O$ concentration histories. However, there does exist a higher vapor $H_2O$ concentration at the bottom of the insulation than at the top during most of this typical winter day, which is the opposite of what occurs in the summer. This will result in the diffusion of vapor $H_2O$ upward toward the top of the batt, and hence, should increase the heat loss from the living space. This is clearly seen in the heat flux histories of Fig. 11.

Illustrated in Fig. 11 are the measured total heat flux history, the predicted dry heat flux history, and the predicted moist heat flux history. Figure 11 shows that the experimental data and two numerical models all predict that heat is lost (positive flux) during the entire day. The greatest loss is during the early morning hours ($t < 400$ min). The moist model predicts a slightly higher heat loss during the early morning hours as compared to the dry model; this is due to the upward diffusion of $H_2O$ vapor. Both models are somewhat lower than the experimental data in the early morning hours. However, after the early morning hours the agreement among the experimental data, dry model, and moist model is quite good. The integrated heat flux values over the entire 24-h period are shown in Table 2. This data shows that the moisture accounts for an increase of about 2.5% as compared to the dry model. The moisture numerical model is seen to differ with the experimental data by 6%. The presence of moisture for these winter conditions shows that moisture does result in greater heat losses, but that these losses are not large for Northern Mississippi. However, these winter heat losses associated with the presence of moisture could be greater for other geographic regions where high wintertime moisture conditions occur.

Depicted in Fig. 12 are the dimensionless spatial vapor $H_2O$ concentration profiles. The profiles at $t = 435$, 600, and 1200 min show a monotonic behavior as vapor $H_2O$ diffuses from the substrate to the top of the insulation. During the peak solar heating portion of the day ($t = 885$ min) the vapor $H_2O$ concentration is essentially constant with a slightly increasing trend; all these spatial profiles are consistent with the boundary concentrations depicted in Fig. 4. Shown in Fig. 13 are the bound $H_2O$ dimensionless concentration profiles. The colder top of the insulation has a higher concentration of bound $H_2O$ than does the warmer bottom of the insulation where $H_2O$ has been desorbed due to the higher temperatures.

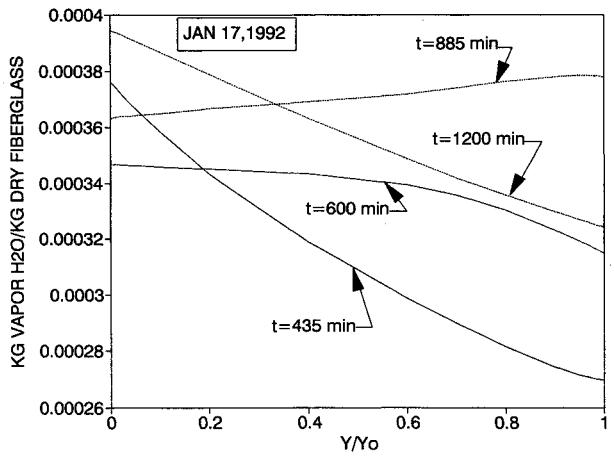


**Fig. 12 Spatial vapor $H_2O$ concentration (kg $H_2O$/kg of dry fiberglass) profiles at four times for R19STD insulation.**

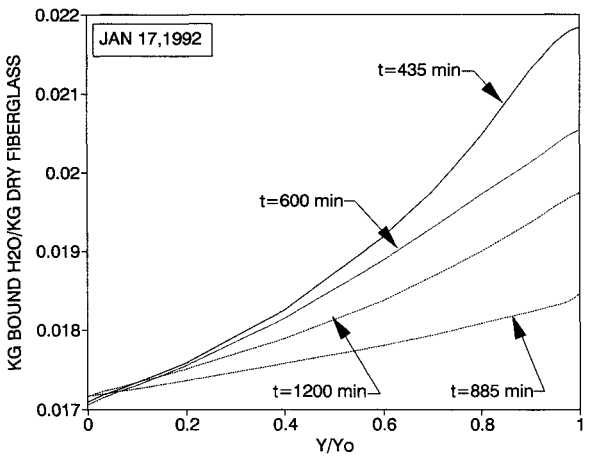


**Fig. 13 Spatial bound $H_2O$ concentration (kg $H_2O$/kg of dry fiberglass) profiles at four times for R19STD insulation.**

### Fall Conditions

Fall conditions correspond to the data recorded during the 24-h time period of October 8, 1992. The appropriate temperature-time histories and relative humidity time-histories plots are not included. However, this was a very sunny, mild, and humid day with the roof temperatures not exceeding 100°F, and the relative humidity inside the attic reaching approximately 60%. Using the temperature and relative humidity data, the vapor $H_2O$ dimensionless concentration histories are shown in Fig. 8 for fall conditions. The vapor $H_2O$ concentration histories are similar to those for the spring conditions, but for the fall conditions there is an inversion between the top and bottom of the batt. During the cooling portions of the day the concentrations at the top of the batt are lower than the concentration levels at the bottom. However, during the heating portion of the day ($500 < t < 900$ min) an inversion takes place, causing the concentrations at the top of the batt to become higher than at the bottom. Figure 14 shows the comparisons of the experimental data, dry, and moist models. As seen in Fig. 14, the numerical models follows the experimental data very good. The dry model tends to deviate from the experimental data and moist model during the heating portion of the day; this implies that the presence of moisture makes a significant increase in the transfer of heat into the living space. Shown in Table 2 are the integrated heat fluxes for the experimental data, moist and dry models. From Table 2 it can be seen that the presence of moisture has resulted in a 16.7% increase in the heat transfer as compared to the dry model during the heating portion of this fall day. The moist

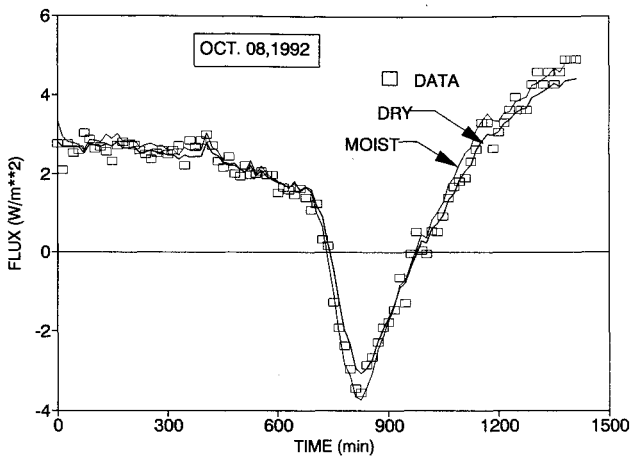


**Fig. 14 Substrate measured heat flux-time and predicted heat flux-time histories for both moist and dry cases for R19STD insulation.**

model is shown to agree within about 1% of the integrated experimental data.

## Summary and Concluding Remarks

A numerical model has been presented which models the coupled radiative, conductive, and mass transfer associated with the total heat transport in low-density attic residential fiberglass insulation. The heat transfer was modeled for typical seasonal conditions in North Mississippi. For the typical summer, spring, winter, and fall conditions it was shown that the presence of moisture transport in the attic resulted in an increased heat transfer to the living space in summer, spring, and fall, and an increased heat loss from the living space in winter. The impact of moisture was found to be most significant for the spring, summer, and fall seasonal conditions. However, the presence of moisture was seen to hurt energy conservation in all seasonal conditions as compared to the dry insulation case. The moisture numerical model was shown to agree well both quantitatively and qualitatively with the measured experimental heat flux data. The numerical model is a useful tool for understanding and predicting the performance of a wide variety of fiberglass insulation scenarios.

Experimental data were obtained from the attic of an occupied North Mississippi residential home. The experimental data included the relative humidities and temperatures at the top and the bottom of the fiberglass insulation batt. These experimental data were employed as the boundary conditions in the numerical model. In addition, the total heat flux at the bottom of the insulation was measured and used to verify the present model. The thermal data were recorded every 15 min using a HP 3582A data acquisition system. Temperatures were measured with type-J thermocouples. Relative humidities were measured with Hycal CT-829-A-RX temperature-compensated relative humidity meters. Heat fluxes were measured with the Hycal BI-7-20-WP-J-X-X6 high-sensitivity heat flux meters; the heat flux meters were calibrated by Holometrix, Inc. The heat flux meters were located at the interface between the fiberglass batt and the gypsum board at the substrate.

## Acknowledgments

The authors wish to acknowledge the support of the Department of Energy EPSCoR program sponsored under Grant DE-FG02-91ER75660. The authors would also like to acknowledge the support of the National Science Foundation for the equipment purchased under Award 8905471.

## References

[1]Fairey, P., Keretecioglu, A., Vieira, R., Swamy, M., and Chandra, S., "Latent and Sensible Load Distributions in Energy Efficient and Passively Cooled Residences," Florida Solar Energy Center, Gas

Research Inst., Contract 5082-243-0727, Cape Canaveral, FL, Aug. 1985.

[2]Rish, J. W., and Roux, J. A., "Heat Transfer Analysis of Fibrous Insulations with and Without Radiant Barriers for Summer Conditions," *Journal of Thermophysics and Heat Transfer*, Vol. 1, No. 1, 1987, pp. 43–49.

[3]Yeh, H. Y., and Roux, J. A., "Spectral Radiative Properties of Fiberglass Insulation," *Journal of Thermophysics and Heat Transfer*, Vol. 2, No. 1, 1988, pp. 75–81.

[4]Yajnik, S., and Roux, J. A., "Determination of Radiative Properties of Fiberglass and Foam Insulations," Oak Ridge National Lab., Sub/86-55930/1, Oak Ridge, TN, Dec. 1987.

[5]Eckert, E. R. G., and Faghri, M., "A General Analysis of Moisture Migration Caused by Temperature Differences in an Unsaturated Porous Medium," *International Journal of Heat and Mass Transfer*, Vol. 23, Dec. 1980, pp. 1613–1623.

[6]Huang, C. L. D., "Multi-Phase Moisture Transfer in Porous Media Subjected to Temperature Gradient," *International Journal of Heat and Mass Transfer*, Vol. 22, Sept. 1979, pp. 1295–1307.

[7]Kumaran, M. K., "Comparison of Simultaneous Heat and Mass Transport Through Glass-Fibre and Spray-Cellulose Insulations," *Journal of Thermal Insulation*, Vol. 12, July 1988, pp. 6–16.

[8]Kumaran, M. K., and Mitalas, G. P., "Simultaneous Heat and Moisture Transport Through Glass Fibre Insulation: An Investigation of the Effect of Hygroscopicity," *ASME Winter Annual Meeting, Solar Energy Technology—SED*, Vol. 4, 1987, pp. 1–4.

[9]Tao, Y.-X., Besant, R. W., and Rezkallah, K. S., "Unsteady Heat and Mass Transfer with Phase Changes in an Insulation Slab: Frosting Effects," *International Journal of Heat and Mass Transfer*, Vol. 34, No. 7, 1991, pp. 1593–1603.

[10]Tao, Y.-X., Besant, R. W., and Rezkallah, K. S., "Transient Thermal Response of a Glass-Fiber Insulation Slab with Hygroscopic Effects," *International Journal of Heat and Mass Transfer*, Vol. 35, No. 5, May 1992, pp. 1155–1167.

[11]Tao, Y.-X., Besant, R. W., and Simonson, C. J., "Measurement of the Heat of Adsorption for a Typical Fibrous Insulation," ASHRAE Transactions Annual Meeting, June 1992.

[12]Hansen, K. K., "Sorption Isotherms," Building Materials Lab., Dept. of Civil Engineering, Technical Univ. of Denmark, Ottawa, Ontario, Canada, 1985.

[13]Gorthala, R., Roux, J. A., and Fairey, P. W., III, "Combined Conduction, Radiation Heat Transfer and Mass Transfer in Fibrous Attic Insulations," *Insulation Materials: Testing and Applications, 2nd Volume, ASTM STP 111*, American Society for Testing and Materials, Philadelphia, PA, 1991, pp. 371–386.

[14]Hust, J. G., Callanan, J. E., and Sullivan, S. A., "Specific Heat of Insulations," *Thermal Conductivity 19*, edited by D. W. Yarbrough, Plenum Press, New York, 1988, pp. 533–550.

[15]Roux, J. A., Smith, A. M., and Todd, D. C., "Radiative Transfer with Anisotropic Scattering and Arbitrary Temperature for Plane Geometry," *AIAA Journal*, Vol. 13, No. 9, 1975, pp. 1203–1211.

[16]Patankar, S. V., *Numerical Heat Transfer and Fluid Flow*, Hemisphere, Washington, DC, 1980.

[17]Gilliland, E. R., "Diffusion Coefficients in Gaseous Systems," *Industrial and Engineering Chemistry*, Vol. 26, 1934, p. 681.

[18]Langlais, C., Hyrien, M., and Klarsfeld, S., "Moisture Migration in Fibrous Insulating Materials Under the Influence of a Thermal Gradient and Its Effect on Thermal Resistance," *Moisture Migration in Buildings*, American Society for Testing and Materials STP 779, 1982, pp. 191–206.